Pre-print of a published manuscript

Application of massive laser shock processing for improvement of mechanical and tribological properties

Uroš Trdan, Michal Skarba, Juan A. Porro, José L. Ocaña, Janez Grum

DOI: https://doi.org/10.1016/j.surfcoat.2018.02.084
Published in: Surface & Coatings Technology, Volume 342, May 2018, Pages 1-11

Received: 15 November 2017
Accepted: 21 February 2018

Application of massive laser shock processing for improvement of mechanical and tribological properties

Uroš Trdan [a*], Michal Skarba [b], Juan A. Porro[c], José L. Ocaña [c], Janez Grum [a]

[a] University of Ljubljana, Faculty of Mechanical Engineering, Askerceva 6, 1000 Ljubljana, Slovenia
[b] Slovak University of Technology in Bratislava, Vazovova 5, SK-81243 Bratislava, Slovakia
[c] UPM Laser Centre, Polytechnical University of Madrid, Ctra. Valencia, k.m. 7.3, 28031 Madrid, Spain

uros.trdan@fs.uni-lj.si, michal.skarba@stuba.sk, japorro@etsii.upm.es, jlocana@etsii.upm.es, janez.grum@fs.uni-lj.si

*Corresponding author: Assist. Prof. Uroš Trdan, PhD.
Email: uros.trdan@fs.uni-lj.si
Tel.: +386 1 477 1432
Submitted to: *Surface and Coatings Technology*
Date: November 15 2017

Abstract

The present paper aims to investigate topographical, microstructural, mechanical and tribological behaviour of precipitation hardened Al alloy subjected to massive laser shock processing (LSP) without protective coating at 2500 pulses/cm², using three beam diameters. Wear tests under dry sliding conditions resulted in severe wear, whereas the main wear mechanisms were adhesion accompanied by abrasive wear. Nevertheless, LSP with optimal processing parameters reduce the friction coefficient and wear rate with lower degrees of adhesion and abrasion inside the wear track in comparison to the untreated sample. The enhanced tribological performance is attributed to the positive influence of LSP induced surface topography, surface compressive residual stresses (RS) and dense dislocation arrangements, as the result of high-pressure shock waves. Nonetheless, due to the narrow window of optimal parameters reduced wear resistance as a consequence of undesired thermal/softening effect due to laser ablation and melting was detected with non-optimal processing parameters.

Keywords: Laser shock processing; Aluminium alloy; Wear, Microhardness; Residual stress; Microstructure.

1. Introduction

Despite the fact that laser processing technologies belong to a green manufacturing branch and that aluminium and its alloys are the third most commonly used commercial engineering materials, a constant demand towards higher efficient surfaces, lower and cleaner production costs with lower waste gas emissions remains. Among the products within the 6xxx series aluminium alloys, AA6082 is regarded as a high (medium-high) strength alloy, which contains high numbers of intermetallic second-phase particles, ranging up to 10 μm, i.e. spherical α-$Al_{12}(Fe, Mn)_3Si$, β-Al_5FeSi, and β-Mg_2Si in the form of plates or cubes [1]. However, the predominant nano-precipitate in the peak-aged condition contributing the most to the increase in material hardness and strength is the β″ phase (Mg_5Si_6) [2]. Nevertheless, despite the fact that the age hardenability of Al–Mg–Si alloys is high due to excess amounts of silicon and magnesium, which enhances the precipitation kinetics during heat treatment, the major disadvantage is insufficient wear resistance [3].

According to Sánchez-Santana et al. [4] wear can be regarded (along with fatigue and corrosion) as one of the three most common problems found in industry, leading to the replacement of industrial parts and components, due to reduced operating efficiency, increased loss of power, oil consumption, etc. Ductile materials, such as aluminium alloys under dry sliding conditions, usually experience severe wear; however, it is far from clear which aluminium alloy would offer the best wear resistance [5]. In fact, as Ghazali et al. [6] suggested it is not clear if the wear resistance scales with the starting hardness of the alloy, which would suggest that a precipitation-hardened matrix would be optimum, or whether it is the work-hardening characteristics that are more important.

Over the previous two decades laser shock processing (LSP) has been recognized as an advanced, effective, fast emerging severe plastic deformation (SPD) technology which has been successfully applied to various materials to impart compressive residual stresses, various high-density dislocation configurations, grain refinement, improved fatigue, corrosion and wear resistance [7][8][9][10][11][12][13][14]. Authors [7][10] have confirmed nanocrystalline structures with refined grains, dense dislocation walls and dislocation cells in the material surface as a consequence of laser-induced shock waves propagating into material. Moreover, it has been shown [11] that LSP with a sacrificial protective layer is a reliable and precise surface texturing technique for the fabrication of surface microdents, which may act as lubricant reservoirs to reduce friction and wear in contact applications. Kumar et al. [12] have also confirmed that LSP with optimized laser fluence can improve wear resistance by as much as 91 % compared to an untreated sample. On the contrary, Hatamleh et al. [14] reported only marginal improvement in wear of laser shock processed stir-welded 2195 Al alloy.

LSP also possess important environmental benefit over conventional SP process, with lower material/energy consumption during the peening process, with as much as 55% lower environmental impacts [15]. Moreover, it was pointed out that LSP has close-to-zero particulate emissions, hence greatly improves the indoor air quality and, thus reduces occupational health risks. However, the same authors argued that with the 'coated' LSP regime the consumption of protective opaque, i.e. aluminium foil present the dominant contributor of energy and material losses across all impact categories.

It should be noted that, according to the availability of different laser sources providing different pulse times and different laser energy over different treatment areas, two main processing regimes for LSP treatments exist, which can be applied either with or without an ablative/protective layer [10]. In the so-called 'high energy + long pulse' regime, pulsed lasers with energy in excess of several tens of joules and interaction times of up to several tens of ns, deliver their energy to broad surface areas (in excess of 10 mm^2). In such way high thermomechanical impulse able to originate the desired residual stress fields on a single pulse-by-pulse basis is provided. This approach demands an additional protective/sacrificial overlay (paint, metallic tape, etc.) at the interaction zone prior to the laser application. The absorbing protective coating enhances the laser radiation absorption and, in turn, prevents thermal effects caused by the relatively long time of contact between the plasma and the treated material.

In contrast to the coated LSP regime, the so-called 'low energy + short pulse' regime was developed in 1995 for nuclear power plants since the process requires neither surface preparation under radiation environment, nor drainage of water in a reactor vessel [16] [17]. In this regime, pulsed lasers with interaction times in the range of several ns and with only mJ-J of energy are applied to smaller surface areas in order to maintain the required threshold energy for the LSP effect. In this case, large areas are covered by a controlled pulse overlapping strategy. At each location of pulse incidence, the effect of pulse overlapping can produce a deep (around or over 1 mm) field of compressive residual stress with very good degree of uniformity and control [18]. In this case (with a comparatively short pulse interaction time), the resulting mechanical and thermal waves applied to the treated material are temporarily uncoupled. With the mechanical wave being applied faster, the residual effects of the subsequent thermal wave are comparatively very small and limited to a narrow zone close to the material's external surface. Hence, the effect of shock waves prevails, producing compressive residual stresses [19].

This is an important feature to be taken into account as it is possible to eliminate the coating layer used in the 'high-energy' approach without any appreciable loss of final surface quality. Moreover, a quality factor due to the stress state uniformity in the component being treated can be provided. Further, protective overlay is a time-consuming affair and it must be applied at the interaction zone prior to the application to prevent the surface from being damaged by the high power laser irradiation. Also, the overlay becomes damaged severely during the LSP process, requiring frequent replacement hence making it slow, less efficient and expensive in industrial applications [20]. It should be noted that the handling system with the low energy, uncoated LSP process to access the target component is simpler since there is no reactive force against laser irradiation, which has confirmed this process to be very practical not only in nuclear facilities but also in other harsh environments necessitating full-remote operation [19]. In view of this, low energy, short pulse, laser shock processing without protective coating controlled by a predefined massive pulse overlapping strategy can be regarded as a very promising, cost-effective and cleaner surface treatment technology.

With this in mind and since there is limited reports on the possible detrimental effect of non-optimal LSP process parameters on wear behaviour, the present work describes the investigation of possible improvements of the surface morphology and tribological behaviour of Al 6082 alloy by massive, uncoated low energy LSP with 2500 pulses/cm², using three beam diameters, i.e. three laser intensities. Tribological behaviour was evaluated using a ball-on-disc tribometer and the wear tracks characterized using a scanning electron microscope (SEM). In addition, the influence of laser shock processing on the surface morphology was characterized using a 3D confocal laser scanning microscope (CLSM) and transmission electron microscope (TEM), whereas the mechanical state was evaluated by microhardness and residual stress by XRD and hole-drilling measurements.

2. Experimental design

2.1 Material and sample preparation

Test samples were sectioned from a 10 mm thick rolled plate of 6082 Al alloy, using a water jet process. The chemical composition (in wt. %) of the material used in this study was 0.87 Si, 0.72 Mg, 0.42 Mn, 0.35 Fe, 0.15 minor elements (Cu, Cr, Ni, Zn, Ti) and Al the rest. The overall heat treatment procedure, T651 (homogenization, solution treatment, aging, etc.), including the subsequent LSP is schematically presented in Fig. 1.

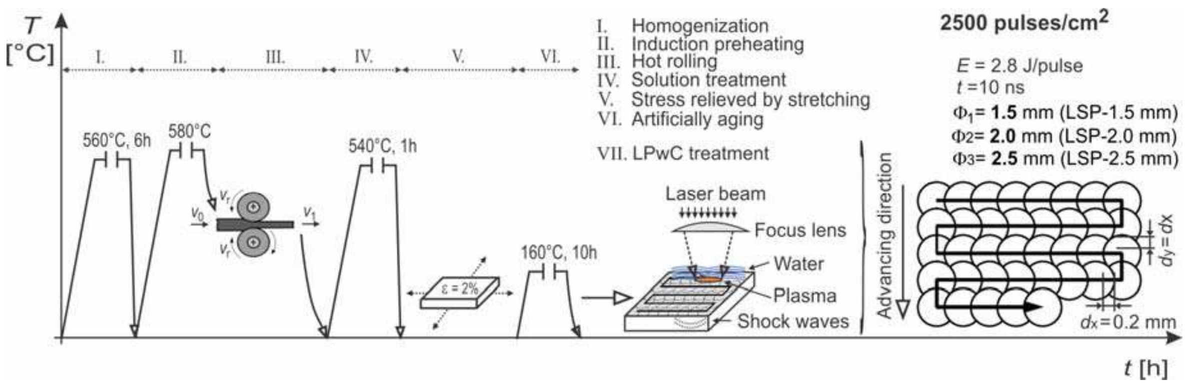

Fig. 1. Schematic presentation of the overall heat treatment and subsequent LSP treatment.

SEM/EDS line analysis (Fig. 2) confirmed the basic Al matrix with fine distribution of intermetallic phases. Results of our previous research [10] confirmed various intermetallic particles in these alloys, i.e. smaller β-Mg_2Si precipitates in the form of plates or cubes and larger α-$Al_{12}(Fe,Mn)_3Si$ intermetallic dispersoids, which are in the length of ~ 4µm.

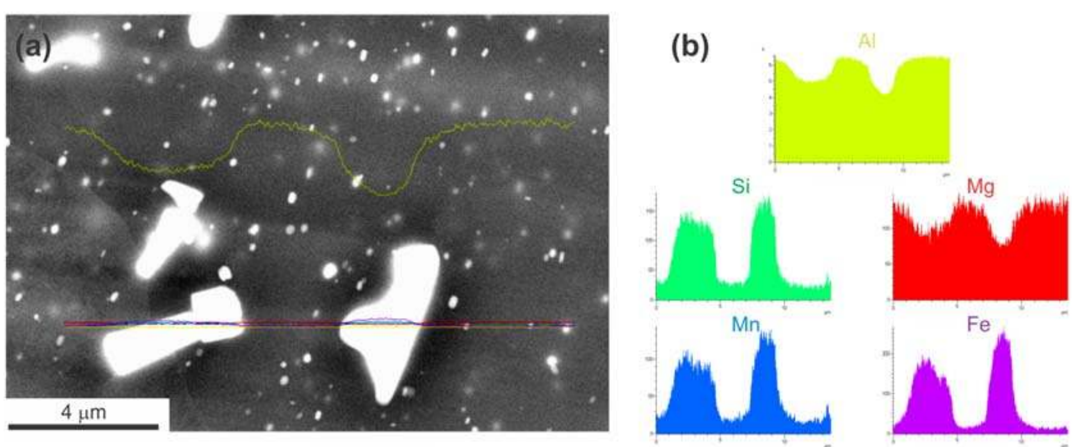

Fig. 2. (a) SEM/BEI microstructure of the base material; (b) EDS line analysis results marked on (a).

Prior to LSP, no additional machining of the samples was carried out. In order to ensure surface uniformity and proper laser laser-beam interactions with the sample surface all samples were thoroughly degreased with acetone and rinsed with de-ionised water, before performing laser processing.

2.2 Laser shock processing

Laser shock processing (LSP) was carried out without any ablative/protective coating in a water confinement regime; whereas laser pulses were overlapped and scanned in a raster-type x-y pattern to completely cover the treated area (Fig. 1). A water jet set up was employed to create a thin water layer with a constant thickness (1–2 mm) and maintain a bubble-free, uniform confinement layer. This enabled plasma confinement during laser–target interaction as well as the replacement of laser ablated particles, ensuring a constant pure laser–matter interaction.

A Spectra-Physics Q-switched Nd:YAG laser source with an irradiation wavelength of 1064 nm, producing 10 ns duration pulses (FWHM), with the maximum laser beam energy of 2.8 J/pulse was used for LSP. The effects of a massive laser shock treatment was investigated at a pulse density of 2500 pulses/cm^2, with a unified overlapping distance between consecutive pulses of 0.2 mm, while the laser beam was constantly perpendicular to the sample surface. Three kinds of beam diameters were chosen, i.e. 1.5 mm (LSP–1.5 mm), 2.0 mm (LSP–2.0 mm), and 2.5 mm (LSP–2.5 mm), which modified surface layers differently due to different peak power density and coverage factors, as shown in Fig. 3.

For each parameter set of the experimental run, two samples were prepared for further analysis; (i) tribological characterization, and (ii) evaluation of surface modifications. In order to investigate the effects of massive LSP on surface integrity, i.e. laser-shock induced surface craters, dislocation configuration, and mechanical properties and its effect on dry-contact wear behaviour, no additional grinding of the treated surface was employed since it would not reflect the real surface condition induced by the laser treatment.

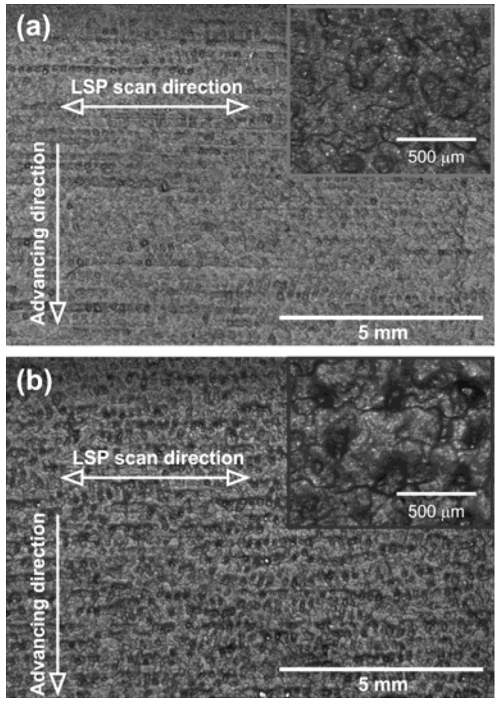

Fig. 3. Surface appearance after LSP with different beam diameters; (a) LSP–1.5 mm and (b) LSP–2.5 mm.

2.3 Surface topography

Topographical analyses were performed using a confocal laser scanning microscope (CLSM) at a wavelength of 405 nm (Zeiss LSM700) to study the influence of massive LSP on the spatial characteristics of the treated surface. Determinations of surface roughness and waviness were obtained using a unified high-pass and low-pass filter with (λ_c = 200 µm).

2.4 Residual stresses and microhardness

Surface transverse σ_{xx} and longitudinal σ_{yy} residual stresses (RS) in regard to the LSP direction (Fig. 1) were determined by a Proto iXRD system with Cr-Kα X-rays (2.291 Å) from the Al{222} diffraction peak located at the angle $2\Theta = 156.31°$ [21][22]. The side inclination method with 9 beta angles with 5° oscillation for each measurement point was adopt, and the $\sin^2\psi$ method with a Gaussian profile fitting was applied for the residual stress analysis. The X-ray elastic constant $S_2/2$ used was 18.56×10^{-6} MPa^{-1}. The focused X-ray beam diameter was set to 2.0 mm.

Depth-resolved RS were measured with a Hole-Drilling measurement equipment and the strain gage CEA-06-062UM-120 (Vishay Intertechnology Inc., Malvern, PA, USA) in accordance with ASTM E 837-08 standard [23] and Vishay Tech Note TN-503-10 [24]. Diameter of the blind hole was measured using Alicona G4 3D Infinite focus measuring (IFM) device, with an optical lateral and vertical resolution of 800 nm and 100 nm, respectively. The final RS in depth-distribution was calculated with the integral method, using H-Drill software, whereas the average standard deviation of the errors in the measured strain values was 4.7 με. Both, hole-drilling technique, its operation principles and parameters of the IFM device have been described in detail in ref. [18].

Near surface micro-hardness measurements prior to and after LSP were carried out on a Vickers Hardness (HV) tester at a constant 200 g load and 20 s load time at the depth 75 µm below the surface, whereas in average five separate measurements for each data point were performed.

2.5 Microstructural observations

Worn surfaces of samples were identified with a Hitachi S-3000N scanning electron microscope (SEM) attached to an Energy Dispersive X-ray spectroscope (EDX). Microstructures of base material (BM) and LSP-treated samples were characterized in the cross-sectional direction using a Jeol 2000-FX transmission electron microscope (TEM), operated at 200 kV. Detailed TEM procedure TEM was described previously in ref. [10].

2.6 Friction and wear behaviour

Tribological behaviour under dry contact conditions was studied in air at an ambient temperature of 23 °C with a Microtest MT/30/NI/LIN tribometer using a ball-on-disc configuration with a rolling ball of AISI 52100 steel (diameter 3 mm). Test parameters were chosen according to the ASTM G99-04 standard [25] as follows: sliding tangential speed 0.0785 m/s, sliding distance 1000 m and a normal load of 5 N, which corresponds to a maximum Hertzian contact pressure of 1.22 GPa (mean value 0.81 GPa).

During the experiments friction coefficient were recorded. Afterwards, additional measurements of the cross-sectional areas for the calculation of the worn volume (area multiplied by the average length of the footprint) were assessed by means of a Leica ICM1000 confocal laser scanning microscope (CLSM) with a wavelength of 635 nm. For each condition, four measurements of the cross-sectional area at different locations of the groove were taken and averaged and specific wear rate K was calculated based on the worn volume.

Moreover, to obtain a further insight about massive LSP effect on wear behaviour additional surface profile, height-difference measurements, i.e. cross-sectional correlations (maximum height & max. depth) measurements and roughness analyses [26][27][28] of the wear track. All measurements were performed using Alicona G4 3D IFM device (using the same parameters as described above), whereas determinations of surface roughness were obtained using a unified high-pass filtration ($\lambda_c = 250$ μm).

3. Results and discussion

3.1 Surface topography

Fig. 4 and 5 show the topographic characteristic of the BM and the LSP sample surfaces, respectively. Since all laser treated samples showed similar topography as the result of massive laser shock processing at 2500 pulses/cm², the sample LSP-1.5 mm (Fig. 5) was chosen as the representative one, whereas the topography results of all samples are given in Table 1. In order to obtain a proper insight about LSP effects on surface topography, analyses were performed only on the laser processed region.

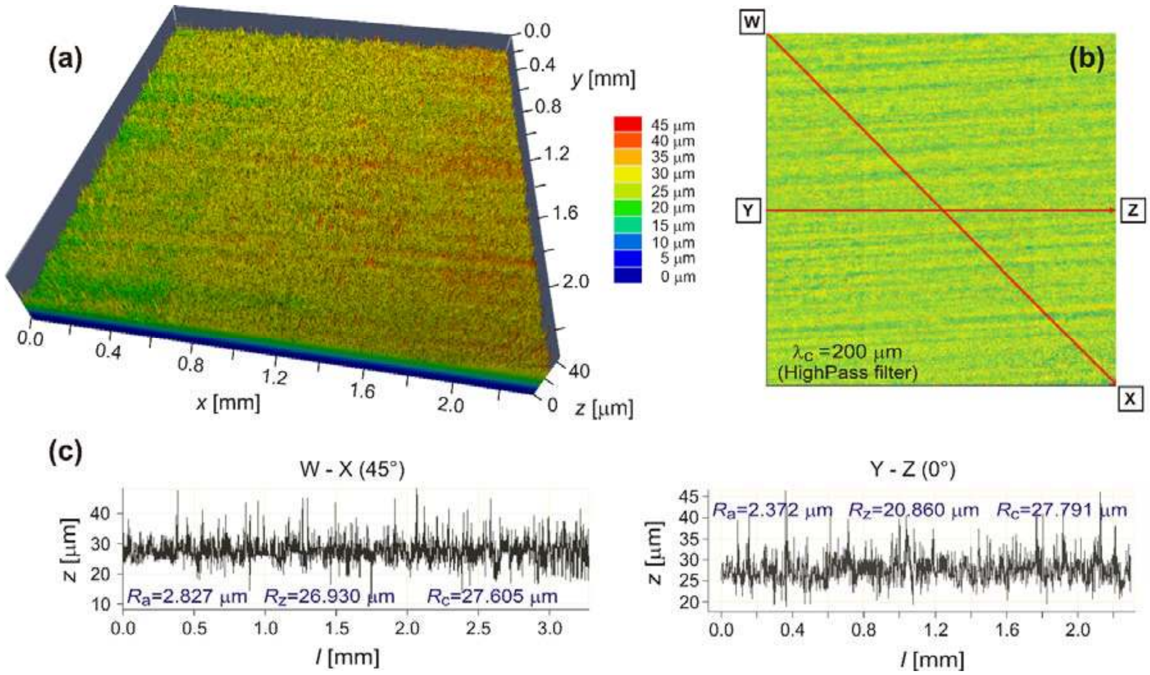

Fig. 4. CLSM topographical analysis of BM sample; (a) 3D image, (b) 2D image after high-pass filtration and (c) topographical line profiles marked in (b).

Topography comparison among these two samples confirms a major influence of preliminary laser treatment, with higher waviness and roughness with the LSP sample. Moreover, the roughness profile values with the BM sample in the directions of 0° and 45° (marked on Fig. 4b) reveals very small differences as a consequence of the rolling (R_a=2.372 µm vs. R_a=2.827 µm). However, after LSP (Fig. 5), the significant anisotropy effect in surface roughness can be seen as a collateral effect of the raster-type laser scan pattern (see Fig. 1 and 3) Here, the R_a value is higher by as much as 43 % in the longitudinal (0°) in comparison to the diagonal (45°) direction, i.e. 3.983 µm vs. 2.784 µm.

In order to obtain further surface texture information and comparison among BM and LSP-treated samples, three 3D amplitude roughness parameters (S_c – mean height of the roughness area; S_a – arithmetical mean deviation of the roughness area and S_z – averaged peak to valley of the roughness area) and three waviness parameters (W_c – mean height of the waviness area;

W_a – arithmetical mean deviation of the waviness area and W_z – averaged peak to valley of the waviness area) were analysed over the complete measured area.

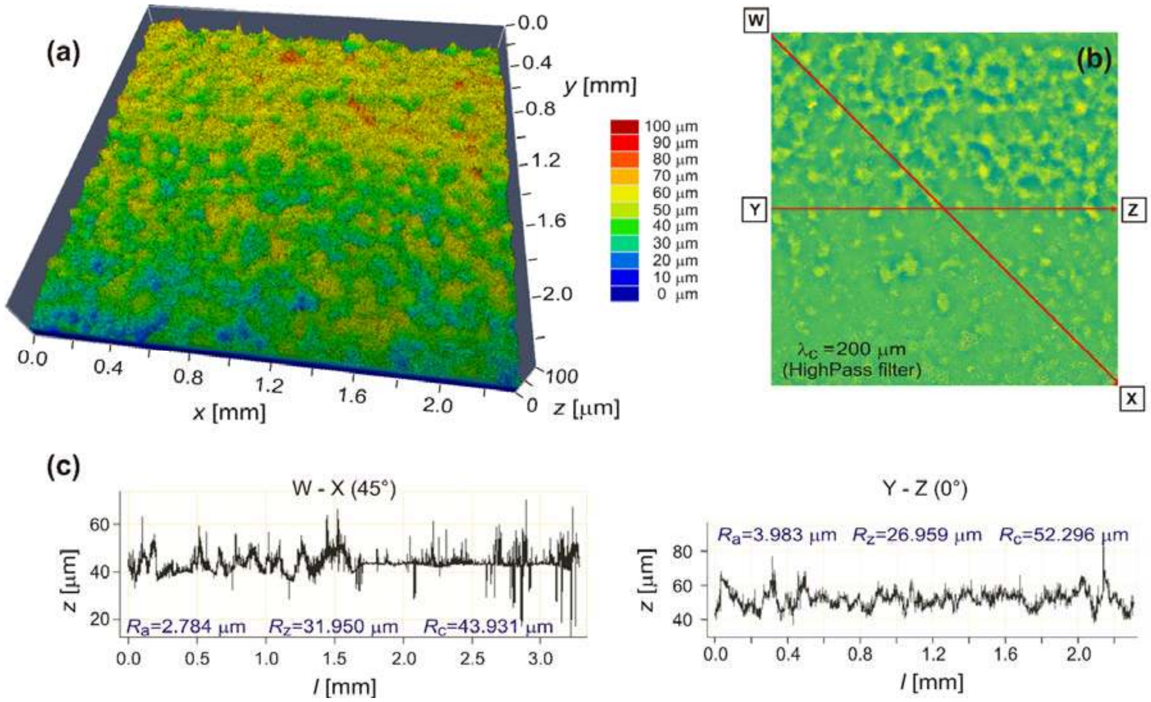

Fig. 5. CLSM analysis of LSP–1.5 mm sample. (a) 3D image, (b) 2D image after high-pass filtration and (c) topographical line profiles marked in (b).

As can be seen from the results in Table 1, the laser beam diameter has a significant effect on the final 3D topography, whereas the lowest roughness and waviness is obtained with the BM sample. With the BM sample roughness S_a, evaluated over the complete measured surface equals to 2.689 μm. After LSP, the roughness S_a increases with increasing beam diameter, i.e. 3.479 μm (LSP–1.5 mm) < 4.374 μm (LSP–2.0 mm) < 6.463 μm (LSP–2.5 mm). Therefore, the S_a parameter is lower by as much as a factor of 1.9 with the sample LSP–1.5 mm in comparison to the sample treated with the largest beam diameter (LSP–2.5 mm). A similar situation can be observed with other 3D amplitude roughness parameters. Moreover, the results confirm that the LSP process modifies the waviness parameters even more. In particular, sample LSP after laser treatment with the largest laser beam diameter reveals a high increase of waviness, exhibiting an almost 35-times higher averaged peak to valley parameter W_z in comparison to the BM sample (68.704 µm vs. 1.986 µm) and a 10-times higher value in comparison to the LSP–1.5 mm sample (W_z=6.646 µm). Hence, the obtained results indicate that the surface topography is indeed sensitive to the laser beam diameter and overlap ratio, expressing a lower degree of asperities (smaller roughness and waviness) with the lowest overlap ratio with the smallest laser beam diameter, and vice versa.

Table 1. 3D CLSM topography (roughness and waviness) results.

Sample	S_c (µm)	S_a (µm)	S_z (µm)	W_c (µm)	W_a (µm)	W_z (µm)
BM	27.860	2.689	48.629	5.240	1.098	1.986
LSP–1.5 mm	48.369	3.479	76.577	9.047	3.011	6.646
LSP–2.0 mm	66.905	4.374	85.514	21.351	8.955	14.334
LSP–2.5 mm	85.777	6.463	94.140	77.388	21.398	68.704

During LSP, expressive surface craters were generated due to numerous laser-beam interactions with the sample surface, producing local surface ablation and plastic deformation induced by multiple laser-induced shock waves at ultra-high strain rates, which can exceed 10^7 s^{-1} [29]. Similar trend of the increased surface topography was reported previously by Yakimets et al. [30], whereas only the changes of wave parameters with unchanged roughness were confirmed. Nevertheless, it should be noted that in their investigation, an ablative protective coating was used, which caused only a mechanical effect due to shock wave propagation.

3.2 Residual stresses and microhardness

In this section residual stresses were investigated since it exist in almost all materials and arise whenever inelastic processes occur [31]. Moreover, the actual sign of residual stresses (tensile/compressive) and their location plays a crucial role on material performance in engineering applications, thus, demands the precise knowledge and control of residual stresses in various applications [32]. Although, recently intensive research efforts have been devoted on downscaling of stress relaxation measurement techniques to a local- /micro-scale by slit milling method using a combination of SEM imaging, FIB milling, and DIC image analysis [31][32][33][34], in this study residual stresses were analysed using a combination of standardized XRD and hole drilling method.

Fig. 6a and b illustrates in-depth residual stress distribution in x (σ_{xx}) and y-direction (σ_{yy}) obtained using the hole drilling technique. Examination of the holes after the drilling (Fig. 6c) confirms good accuracy and stability of the hole drilling equipment even at larger depths, with the average blind-hole diameter of 2.05 ± 0.03 mm.

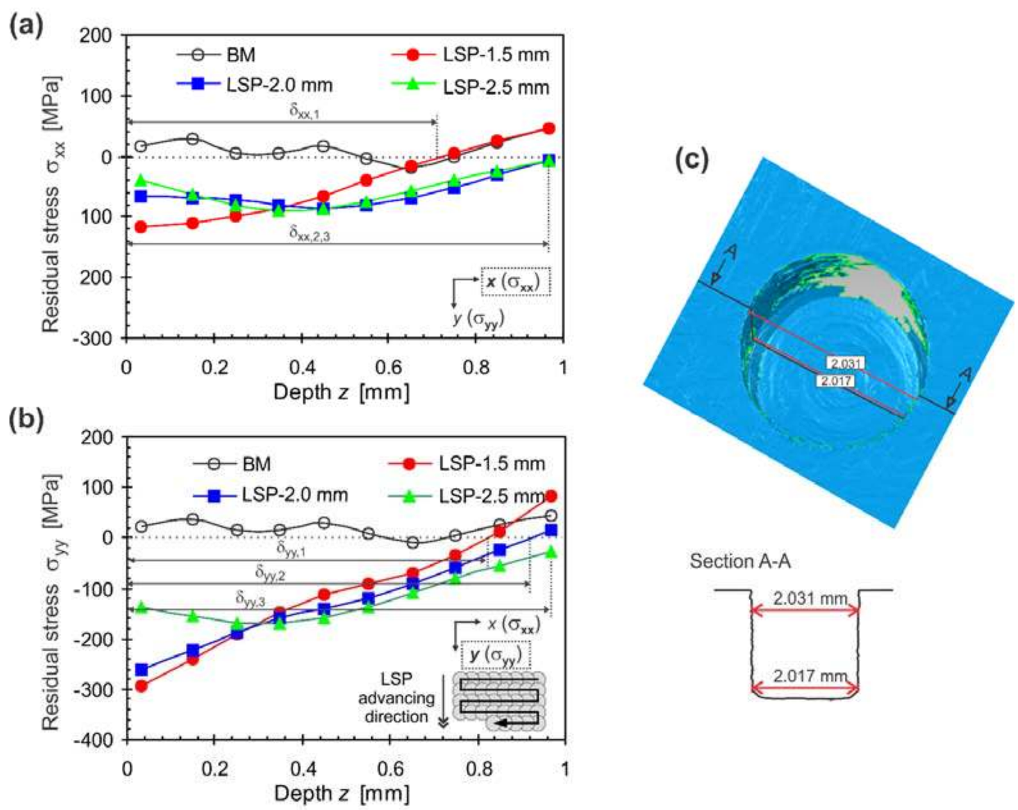

Fig. 6. (a,b) In-depth residual stresses and (c) 3D presentation of the drilled blind-hole and its cross section (*Note*: blank spaces in Fig.6c represent the un-measured points).

The results of the residual stress measurements indicate close to zero stress state with the BM sample. On the contrary, all LSP samples indicate compressive stresses with significantly higher values in the advancing, y-direction (σ_{yy}). Results depict that the magnitude of compressive RS correlates with the magnitude of peak power density and is in the following order: LSP–1.5 mm (–292 MPa) < LSP–2.0 mm (–261 MPa) < LSP–2.5 mm (–138 MPa). As can be seen from Fig. 6b a relatively steep stress gradient is observed where the compressive RS within the first 350 µm increases to ~ -170 MPa. After this region, similar RS distribution can be seen as with the other two LSP samples. However, with larger beam diameter, the penetration depth of compressive RS is higher. Hence, the lowest ($\delta_{xx,1}$ =725 µm) and the highest ($\delta_{xx,3}$ >967 µm) penetration depths of compression in x-direction are obtained with laser beam diameters of 1.5 mm and 2.5 mm, respectively.

It should be noted that compressive RS of -292 MPa and -261 MPa obtained with the samples treated with beam diameter of 1.5 and 2.0 mm in y-direction are very close to the yield strength of the material (320 MPa), indicating that RS are probably overestimated and the actual RS should be lower. Nonetheless, hole-drilling technique provides useable qualitative information about in-depth residual stress distribution [35][36].

Another important factor to be noted from Fig. 6 is quite large differences among RS in the specific direction (σ_{xx} and σ_{yy}) as the collateral effect of the raster laser scan pattern [37]. Nevertheless, it is worth noting that although differences among RS components in a specific direction exist, both stress components are of a compressive character, which could effectively enhance wear resistance.

In order to investigate the possible thermal/softening effect on the very top surface produced during massive uncoated LSP regime, additional XRD RS measurements were performed. Fig. 7 shows a comparison between top-surface RS and near-surface (z = 75 µm) Vickers micro-hardness. Surprisingly, the highest compressive RS are achieved with the sample LSP–2.0 mm treated with middle laser beam diameter (σ_{yy} = -55 ± 11 MPa and σ_{xx} = -22 ± 9 MPa), followed by sample LSP–1.5 mm and LSP–2.5 mm. Results depict larger compressive RS in the y-direction compared to the stresses in x-direction, which is in accordance with the hole-drilling RS results. Further, with sample treated with 1.5 and 2.0 mm laser beam diameter compressive RS are achieved in both directions, indicating sufficient shock waves and work hardening effect, which prevailed over the thermal effect due to laser ablation and melting.

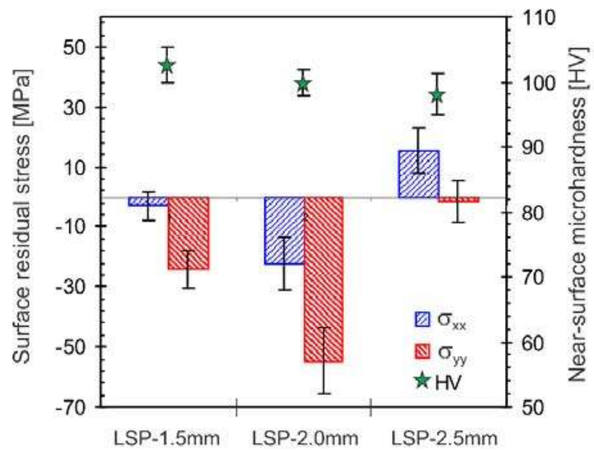

Fig. 7. Comparison of surface residual stress and near-surface micro-hardness.

However, with LSP–2.5 mm sample tensile stresses in the x-direction (σ_{xx} = 15 ± 8 MPa) and near zero RS in the y-direction (σ_{yy} = -1 ± 7 MPa) are obtained. Such results indicate that here the softening/thermal effect prevailed over insufficient mechanical shock wave loading due to low power density and high coverage factor as a consequence of the largest laser spot diameter. Similar results were reported by Gill et al. [20] who investigated the effects of laser shock processing with and without protective coating, where high compressive RS (-550 MPa) with a protective overlay and much smaller compressive stresses (−50 MPa) without a protective coating were confirmed. However, their results depicted tensile RS from the depth of ~5 – 80 µm below the surface which afterwards changed to a compressive state. Our results (Fig. 6 and 7) did not demonstrate this, indicating the important influence of the LSP parameters.

Micro-hardness of untreated material was approximately 94 HV, whereas the highest micro-hardness increase of about + 9% is obtained with the sample LSP–1.5 mm (103 ± 3 HV vs. 94 ± 2 HV). The micro-hardness of other two LSP samples is 100 ± 2 HV and 98 ± 3 HV, respectively. These results indicate correlation with the magnitude of compressive RS in Fig. 6 at the depth of 75 μm, where microhardness was measured. Although, it would be expected that large compressive RS would affect the microhardness on the larger scale, our results indicate only minor increase. Such results are consistent with our previous study [38] and with results reported by Peyre et al. [39], who also reported little improvement in the micro-hardness properties for 7075 Al alloy after laser shock processing compared to shot peened material.

3.3 TEM analysis

Fig. 8 shows the TEM bright field images of the surface layers of untreated and LSP samples. It can be distinctly observed from Fig. 8a that the dislocation density in BM sample is moderately low, with two sets of nano intermetallic particles inside the matrix.

On the contrary, Fig. 8b-d confirms high-density dislocations introduced by laser shock processing. Fig. 8b and c show dense dislocation walls, dislocation tangles and cells having relatively thin walls. Here, only a few dislocation lines were observed, but dislocation pile-ups are formed in the vicinity of the different particles, which seems to act as effective blockers of dislocation movement. Fig. 8b indicates that severe plastic deformation induced by massive LSP impacts promoted in considerable increase in dislocation density, as well as in the formation of dislocation networks and dislocation cell structures, which can lead to refined and eventually to ultra-fine and nano-grains [40]. Results of our previous study [10] indicate that dislocation slip is the main factor of the grain refinement mechanism during LSP as a result of repetitive laser-induced shock waves at the treated surface. Based on the comprehensive TEM analysis and dislocation density evaluation, the grain refinement mechanism has also been proposed therein.

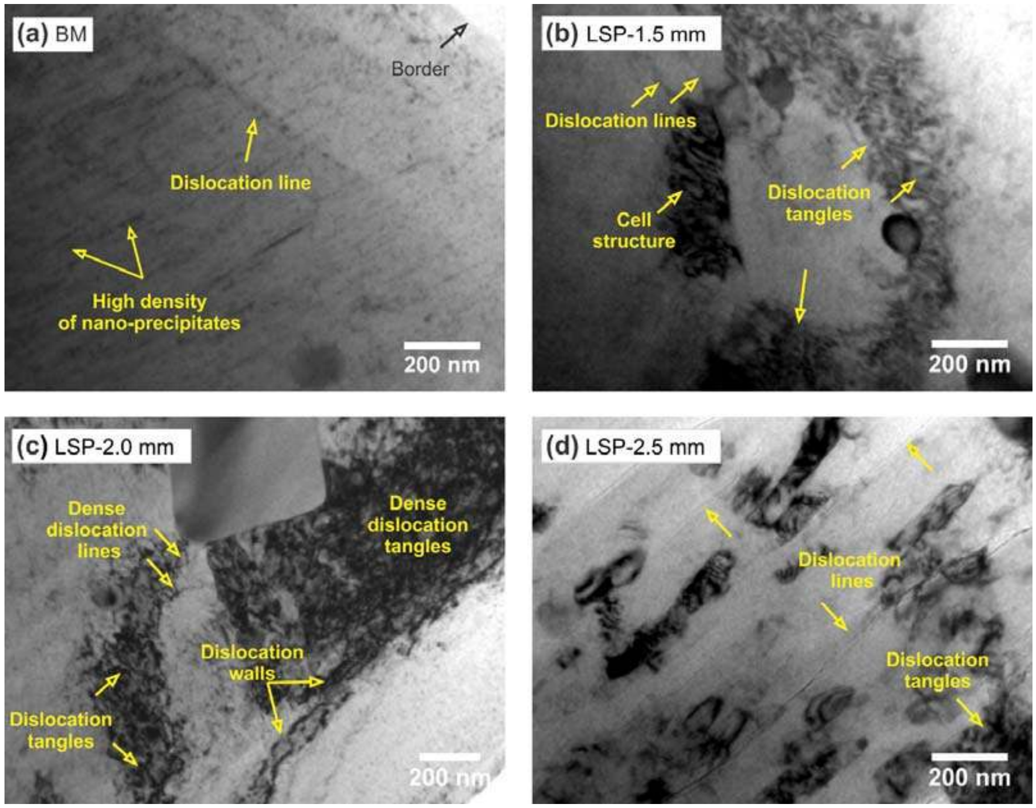

Fig. 8. TEM bright field observations of various samples: (a) BM, (b-d) LSP samples treated with different laser beam diameters.

Moreover, current and previous TEM observations revealed no effect of LSP on precipitation kinetics, its distribution and size which is common with conventional shot peening process. For example, Noordhuis and De Hosson [41] report obvious very fine dispersion of silicon in aluminium of laser melted and shot peened eutectic aluminium-silicon (Al-12Si) alloy with formation of small silicon precipitates, which lead to a further hardness increase. In contrast, our results did not demonstrate this, which is in good correlation with obtained hardness results, since the nano-size β″ phase (Mg_5Si_6) precipitates contributes the most to the increasing strength of Al-Mg-Si alloys [2][42]. Hence, finer or denser distribution of β″ nano-size precipitates reflects in greater hardness and strength of such Al-alloy [10]. Fabbro et al. [43] attributed this differences (SP vs. LSP) to three interactive factors: (1) shock duration is very small, (2) compared to the SP process, no contact deformation or Hertzian loading occurs, and (3) impact pressures are usually much lower than those from the SP process. Nevertheless, the same authors confirmed more than two times higher fatigue life after laser shock processing compared to the shot peening, in which higher surface embrittlement and surface roughening promoted more rapid crack development.

However, in the case of the LSP–2.5 mm sample (Fig. 8d) the situation is different. Here, TEM analysis shows only the presence of dislocation lines and the presence of nano-particles, of which many have planar defects as a result of thermal effect, producing tensile RS (Fig. 7). This phenomenon is most likely associated with nano-particles deposition on top of the underlying matrix during LSP treatment, where after surface ablation shock waves re-deposit these particles on the matrix [20]. However, this is consistent only with LSP–2.5 mm sample treated with the largest beam diameter and the highest overlapping ratio and is not the case with other two LSP samples.

3.4 Friction and wear

Fig. 9 shows the real time friction coefficient variation of BM and LSP samples during wear tests with a contact force of 5N and speed of 0.0785 m/s. From the global friction coefficient evolution for the pair of 6082 Al alloy–AISI 52100 stainless steel ball (Fig. 9a), it can be noted that all samples exhibited a similar trend, with a certain degree of oscillation.

By examining the diagram of the friction coefficient vs. sliding distance, it can be seen that the friction coefficient stabilizes quickly after the start (running-in-period). Afterwards, active friction is observed showing the approximately linear function of the sliding distance. At the beginning of the steady state period (~ 100m), the friction coefficient was found to be approximately 0.4 and 0.3 for the BM and LSP samples, respectively. With further sliding distance, the friction coefficient show a constant increase with a certain degree of oscillations, associated with a stick-slip phenomenon as adhesion wear takes place, due to junction formation and interlocking of asperities between mating surfaces and progressive degradation of the sample surface. Wear particles which are generated begin to plough into the surface, indicating steady weight loss of the tribosystem.

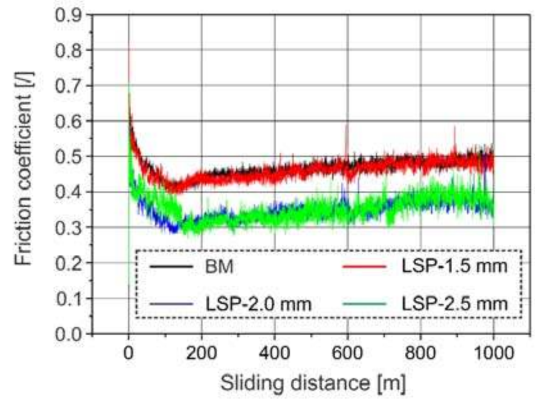

Fig. 9. Friction coefficient as a function of sliding distance.

Nevertheless, Fig. 9 shows that, in comparison to the BM, LSP produce a lowering of the global friction coefficient under dry contact conditions. After ~700 m, all samples show almost constant friction, indicating that wear particles inside the wear track are balanced by wear particles leaving the wear track. The average friction coefficient at the end of the test at 1000 m sliding distance was 0.51 for the BM and in the range of 0.36 – 0.48 for LSP samples. LSP–1.5 mm sample shows similar friction to the BM sample most likely due to the lower surface roughness and waviness compared to the other two LSP sample (Table 1), which reflect in less contact points of asperities resulting in increased contact pressure and coefficient of friction.

Fig. 10 shows an example of the typical wear pattern and an obtained 3D CLSM profile, which was employed to determine worn volumes. Visual inspection revealed no visible damage on the AISI52100 ball surface, due to its much higher hardness. Thus, the wear of the ball was neglected. In order to obtain accurate readings measurements of the wear volume were taken at four different locations along the wear track, and the average value along with the standard deviation was calculated. After determination of the worn volumes, specific wear rates of the samples were calculated, and wear scars were evaluated via SEM/SEI analysis to determine whether severe or mild wear occurred.

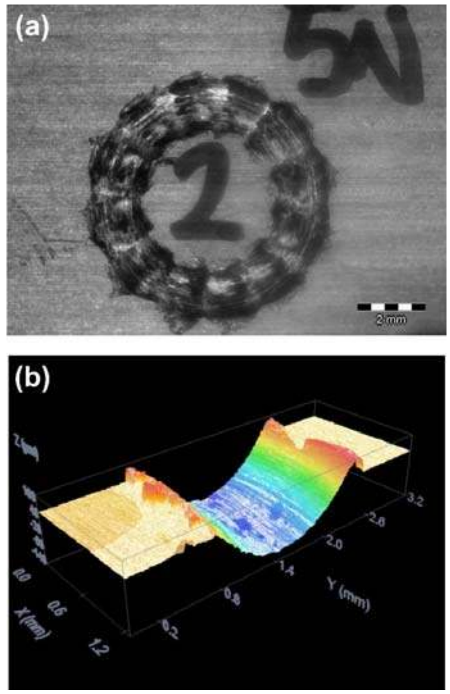

Fig. 10. Typical wear scar (a) and 3D CLSM wear scar profile (b).

Measured wear volume and calculated values of the specific wear K rate (worn volume (mm^3) divided by the product of load (N) and total sliding distance (m)) of untreated and LSP samples are given in Table 2. The specific wear rate of BM sample ($4.08 \pm 0.83 \times 10^{-4}$ mm^3/Nm) is 12 % higher in comparison to the sample LSP–2.0 mm ($3.64 \pm 0.59 \times 10^{-4}$ mm^3/Nm), which exhibited the lowest wear among all samples. Nonetheless, it should be noted that values of specific wear rate greater than 2×10^{-4} mm^3/Nm indicate that sever wear occurred with all tested samples [44][45]. As expected, the highest wear rate ($K = 4.09 \pm 0.86 \times 10^{-4}$ mm^3/Nm) was achieved with LSP–2.5 mm sample.

Table 2. Wear volume (W_v) and specific wear rate (K) results.

Sample	W_v (mm^3)	σ (mm^3)	K ($mm^3/N\ m$)	σ ($mm^3/N\ m$)

Untreated	2.041E-03	4.165E-4	4.083E-4	8.331E-5
LSP–1.5 mm	1.959E-03	3.199E-4	3.918E-4	6.398E-5
LSP–2.0 mm	1.820E-03	2.952E-4	3.640E-4	5.904E-5
LSP–2.5 mm	2.045E-03	4.289E-4	4.090E-4	8.578E-5

The higher specific wear rate of the sample LSP–2.5 mm treated with the largest spot diameter is directly associated with the treatment itself, due to the softening effect during laser shock processing. As TEM analysis confirmed local thermal effects with this sample caused the lowest dislocation density inside the Al matrix (Fig. 8d) and tensile surface RS (Fig. 7), which restrained the protective properties above the critical pressure during the wear test as soon as the asperities induced by LSP were worn off.

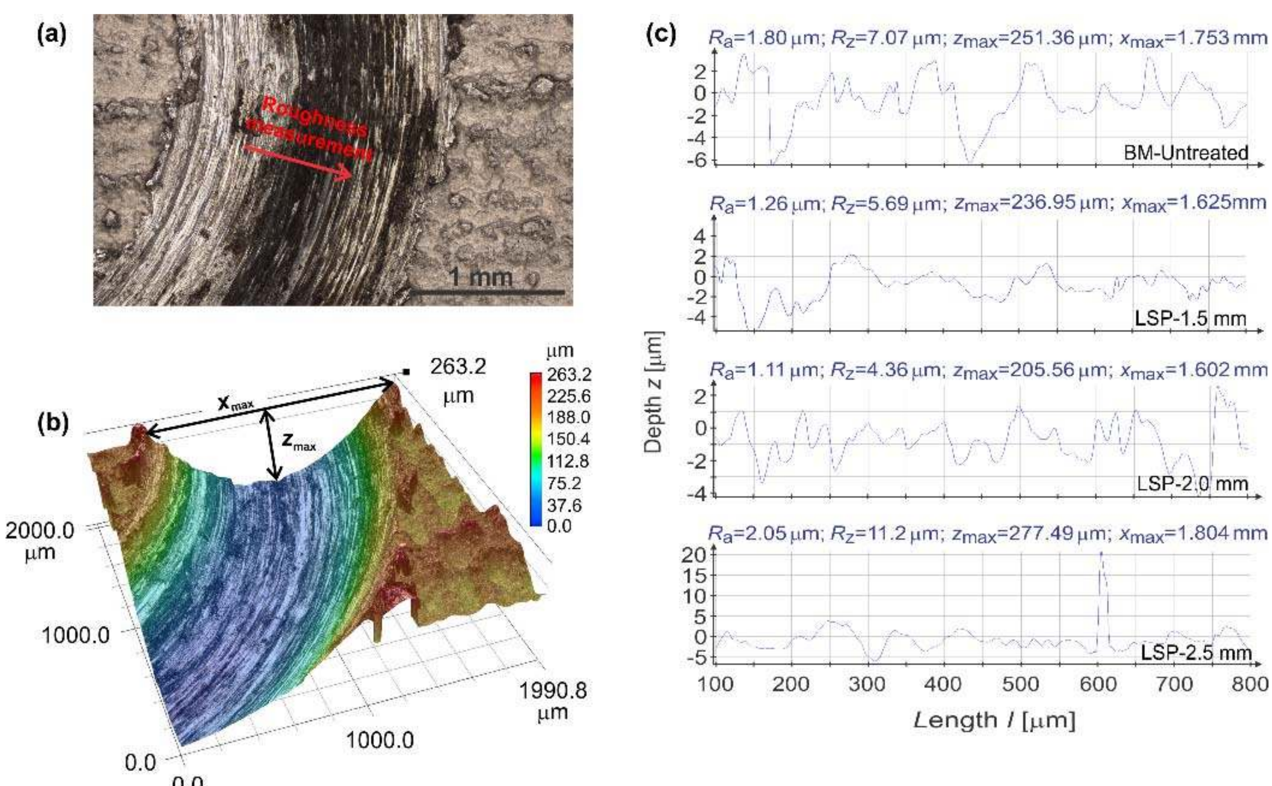

Fig. 11. (a) Schematic presentation of roughness measurement and (b) determination of maximum width and height of the cross sectional profiles of the wear track. (c) surface profiles inside the wear track with given values obtained form the topographical analyses.

Topographical features of the wear scars, i.e. surface profile, cross-sectional measurements maximum height and roughness analyses were additionally studied by IFM microscopy (Fig.11). From the cross sectional profiles (Fig.11b) maximum width (x_{max}) and height (z_{max}) of the wear track were determined. Results from Fig 11c depict perfect correlation with the Wear volume (W_v) and specific wear rate (K) results. Moreover, it is clearly revealed that the largest x_{max} (~1804 μm) and z_{max} (~277 μm) of the wear track was obtained with LSP–2.5 mm sample, which exhibit almost 35% higher maximum height in comparison to the LSP–2.0 mm sample (and z_{max} = ~206 μm) due to occurrence of higher degree of abrasive wear, mainly by a ploughing mechanism. This is additionally confirmed by the roughness results (Fig.11b and c), whereas LSP–2.5 mm sample achieved the highest surface roughness inside the wear track. Results depicts that the roughness R_a inside the wear track is in the following order: LSP–2.0 mm (1.11 μm) < LSP–1.5 mm (1.26 μm) < BM (1.80 μm) < LSP–2.5 mm (2.05 μm). Although, in the case of hard, tough coating (e.g. TiC/a-C nanocomposite coatings) almost linear correlation among wear rate and rate of roughness decrease exists [26], that does not hold true in the case of soft materials. It should be noted that in such tribo-systems (soft Al alloy-hard tool steel) surface asperities are worn off almost instantly during wear at such high maximum Hertzian loading (p_{max} = 1.22 GPa). Hence, compressive residual stresses and refined microstructure seemingly plays a crucial role on wear behaviour.

The above findings are additionally confirmed by SEM/SEI images of the worn surfaces in Fig. 12. It is clear from Figs. 12a and b that the governing wear mechanism with the BM sample is primarily adhesion and delamination by adhesion due to the occurrence of the stick–slip phenomenon resulting in progressive degradation of the surface. SEM analysis of the worn surfaces at higher magnification (Fig. 12b and d) also confirm abrasive wear with many scratches or grooves parallel to each other in the sliding direction in the worn track on both the treated and untreated samples. However, visual inspection in Fig. 12b shows extensive surface damage accompanied by deeper abrasion groove marks on the BM sample, as a result of the agglomeration and compaction of the third-body wear debris generated during the test [45] [46].

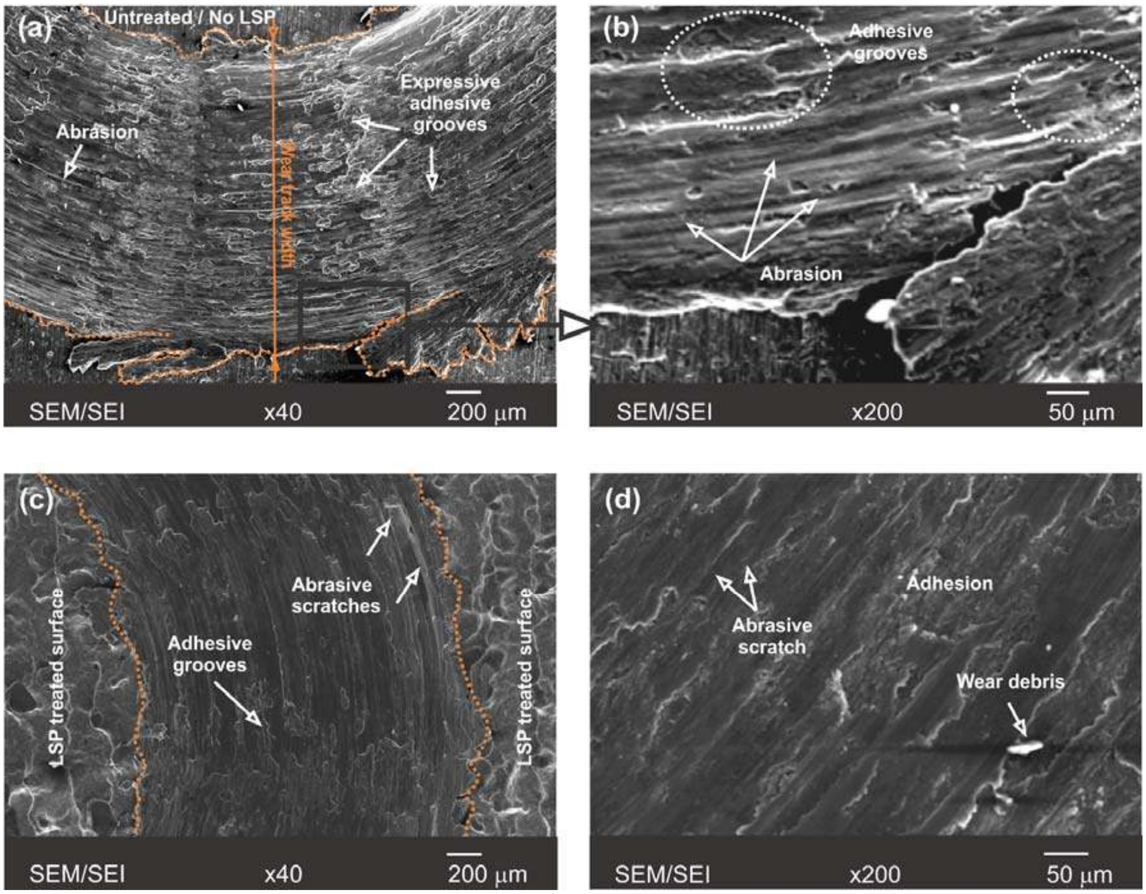

Fig. 12. SEM/SEI images of wear scars; (a-b) Untreated and (c-d) LSP sample treated with 2.0 mm laser beam diameter.

In contrast, after LSP, a smoother surface is obtained, with shallower abrasive marks, with a lower degree of plastic deformation due to high compressive residual stresses induced by the shock waves. Furthermore, the surface condition inside and near the wear track in Fig. 12c shows that the asperities formed during LSP were all removed during the test. Our results are consistent with those reported by Kumar et al. [12], which once again confirm the predominant effect of compressive residual stresses and high density of dislocations induced by the LSP process as soon as the surface asperities due to intense local plastic deformation are worn off.

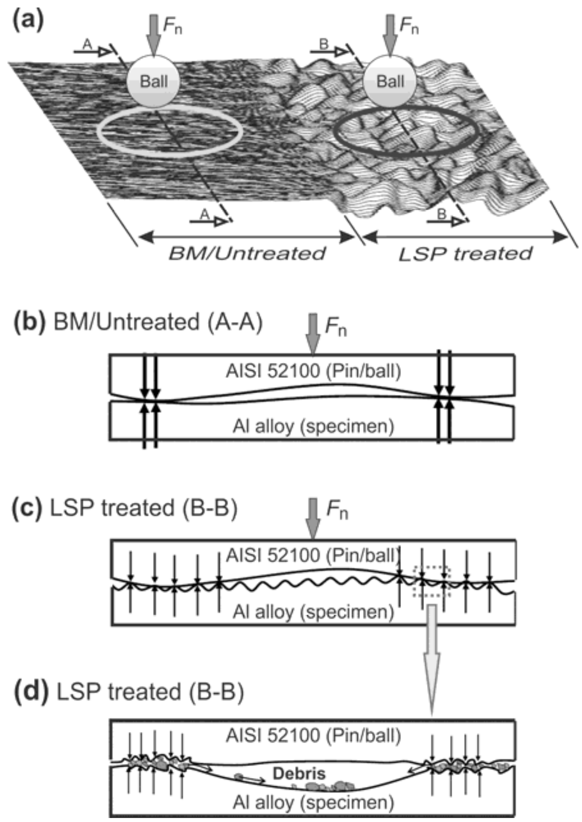

Fig. 13. Schematic presentation of surface topography effect on tribological behaviour under dry contact condition.

The above results confirm that the LSP induced surface asperities (peaks and valleys) and compressive RS beneficially affects the tribological behaviour under dry contact conditions. The schematic presentation in Fig. 13 shows that LSP treatment enables several positive effects on the tribological behaviour:

(i) increasing the number of contact points of asperities and thus decreasing the contact pressure resulting in the reduction of the friction coefficient (Fig. 9);

(ii) increasing the number of interfacial bonds/junctions created during sliding, which would need higher force to break compared to the machined surface;

(iii) neutralizing the degradation process by collecting the wear debris in the valleys of LSP-induced craters, which is consistent with Fig. 12;

(iv) lowering the frictional energy as the asperities are worn off due to high near-surface compressive residual stresses and high density of dislocations, which is consistent with results in Figs. 7-9.

Furthermore, a modified, thicker, and more stable passive oxide film layer generated during LSP treatment could also have contributed to the lowering of friction coefficient and wear. In our previous work [13], XPS analysis confirmed that plasma ablation and shock waves propagation during LSP treatment transforms Al_2O_3 into a more stable oxide form, with higher binding energy, contributing to 7-times higher polarisation resistance R_p and a lower value of double layer capacitance (C_{dl}) than BM sample. Moreover, the deformation response of the asperities peaks in contact before the worn-out also plays a crucial role. Although hardness has a high influence on the surface deformation mode, it seems that surface compressive residual stresses contribute the most. Since the stress originating from sliding is opposed to RS induced by LSP the frictional energy needed for sliding at the beginning of the running-in-period is lower, which is consistent with diagrams in Fig. 9. Our results indicate that surface compressive residual stress plays a crucial role and prevails over surface hardness, indicating higher elastic response of the asperities of the LSP surface.

In addition, under lubricated contact, the positive influence of LSP is even more considerable because surface valleys act as lubricant reservoirs, which help to lubricate contact areas. Hence, it contributes to the generation of hydrodynamic pressure and accordingly separation of materials in contact [47].

5. Conclusions

Dry sliding wear characteristics of BM and LSP samples treated with 2500 pulses/cm², have been investigated. Based on the research conducted, for this specific parameter window used on 6082 Al alloy, the following conclusion can be given:

- Massive LSP can result in surface and in-depth compressive residual stresses with associated high density dislocation structures, accompanied by low, almost negligible increase of surface micro-hardness.
- To minimize surface topography, a smaller laser beam diameter producing a lower overlapping ratio is preferred.
- Massive low energy, LSP was found to be effective in lowering wear rate and friction coefficient by up to 29 %. However, LSP parameters play a crucial role on the tribological properties, which can be even worse than with the BM if the parameters are not optimal and the thermal effect prevails.
- Predominate effect in reducing wear rate are compressive surface RS and high-density dislocation configurations.
- Maximal surface compressive RS were not achieved with the smallest laser beam diameter, i.e. highest power density. Results indicate optimal condition with LSP sample treated with the middle (2.0 mm) laser beam diameter. Here, the highest surface compressive RS, smallest friction coefficient, specific wear rate and wear volume with lowest roughness inside the wear track were achieved, despite lower microhardness compared to the LSP–1.5 mm sample treated with (highest power density).
- The prevailing wear mechanism consists of adhesion, accompanied with abrasion on both the untreated and LSP-treated samples. However, the latter showed superior morphology, with a lower degree of adhesion and abrasion inside the wear track.

Acknowledgments

This work was performed with a financial support from the state budget by the Slovenian Research Agency, Programme No. P2-0270. Part of this work presents the result of the project implementation: CE for development and application of advanced diagnostic methods in processing of metallic and non-metallic materials - APRODIMET, ITMS: 26220120048, supported by the Research & Development Operational Programme funded by the ERDF.

The authors also acknowledge Prof. Jose Luis Ocaña Moreno and Centro Láser UPM (Universidad Politécnica de Madrid,Spain) for laser shock processing and wear measurements.

References

[1] Y, Birol, The effect of processing and Mn content on the T5 and T6 properties of AA6082 profiles, J. Mater. Process. Technol. 173 (2006) 84–91.

[2] M. Cabibbo, S. Spigarelli, E. Evangelista, A TEM investigation on the effect of semisolid forming on precipitation processes in an Al–Mg–Si alloy, Mater. Charact. 49 (2003), 193–202.

[3] C.S. Ramesh, A. Ahamed, Friction and wear behaviour of cast Al 6063 based in situ metal matrix composites, Wear 271 (2011), 1928– 1939.

[4] U. Sánchez-Santana, C. Rubio-González, G. Gomez-Rosas, J.L. Ocaña, C. Molpeceres, J. Porro, M. Morales, Wear and friction of 6061-T6 aluminum alloy treated by laser shock processing. Wear 260 (2006) 847–854.

[5] C. Perrin, W.M. Rainforth, Work hardening behaviour at the worn surface of Al-Cu and Al-Si alloys. Wear 204 (1997) 171-179.

[6] M.J. Ghazali, W.M. Rainforth, H. Jones, The wear of wrought aluminium alloys under dry sliding conditions, Tribol. Int. 40 (2007) 160–169.

[7] S. Lou, Y. Li, L. Zhou, X. Nie, G. He, Y. Li, W. He, Surface nanocrystallization of metallic alloys with different stacking fault energy induced by laser shock processing, Mater. Des. (2016) 104, 320-326.

[8] P. Peyre, L. Berthe, V. Vignal, I. Popa, T. Baudin, Analysis of laser shock waves and resulting surface deformations in an Al–Cu–Li aluminum alloy,2012 J. Phys. D: Appl. Phys. (2012) 45 335304.

[9] D. Karthik, S. Arul Xavier Stango, U.Vijayalakshmi, S.Swaroop, Electrochemical behavior of laser shock peened Inconel 625 superalloy, Surf. Coat. Technol. 311 (2017), 46–54.

[10] U. Trdan, M. Skarba, J. Grum, Laser shock peening effect on the dislocation transitions and grain refinement of Al–Mg–Si alloy, Mater. Charact. 97 (2014) 57–68.

[11] Y.B. Guo, R. Caslaru, Fabrication and characterization of micro dent arrays produced by laser shock peening on titanium Ti-6Al-4V surfaces, J. Mater. Process. Technol. 211 (2011) 729-736.

[12] D. Kumar, S.N. Akhtar, A.K. Patel, J. Ramkumar, K. Balani, Tribological performance of laser peened Ti–6Al–4V, Wear 322-323 (2015) 203–217.

[13] U. Trdan, J. Grum, Evaluation of corrosion resistance of AA6082-T651 aluminium alloy after laser shock peening by means of cyclic polarisation and ElS methods, Corros. Sci. 59 (2012) 324–333.

[14] O. Hatamleh, J. Smith, D. Cohen, R. Bradley, Surface roughness and friction coefficient in peened friction stir welded 2195 aluminum alloy, Appl. Surf. Sci. 255 (2009) 7414–7426.

[15] F. Zhao, W.Z. Bernstein, G. Naik, G.J. Cheng, Environmental assessment of laser assisted manufacturing: case studies on laser shock peening and laser assisted turning, Journal of Cleaner Production 18 (2010) 1311-1319.

[16] N. Mukai, N. Aoki, M. Obata, A. Ito, Y. Sano, C. Konagai, Proceedings of the 3rd JSME/ASME International Conference on Nuclear Engineering (Paper No. S404-3), Kyoto, *Japan*, 1995, 1489-1494.

[17] Y. Sano, K. Masaki, T. Gushi, T. Sano, Improvement in fatigue performance of friction stir welded A6061-T6 aluminum alloy by laser peening without coating. Mater. Design 36 (2012) 809–814.

[18] U. Trdan, J.A. Porro, J.L. Ocaña, J. Grum, Laser shock peening without absorbent coating (LSPwC) effect on 3D surface topography and mechanical properties of 6082-T651 Al alloy. Surf. Coat. Technol. 208 (2012) 109–16.

[19] Y. Sano, N. Mukai, M. Obata, M. Yoda, T. Kubo, I. Chida, T. Uehara, H. Kato, S. Shima, Laser peening without protective coating as a surface enhancement technology. Proceedings of 15th International Conference on Nuclear Engineering (paper no.: ICONE15-10812), Nagoya, Japan, 2007 p.p. 1-8.

[20] A.S. Gill, A. Telang, V.K. Vasudevan, Characteristis of surface layer formed on Inconel 718 by laser shock peening with and without a protective coating. J. Mater. Process. Technol. 225 (2015) 463– 472.

[21] A. Lodini, M.E. Fitzpatrick, editors. Analysis of residual stress by diffraction using neutron and synchrotron radiation. London: Taylor & Francis; 2003.

[22] T. Sano,T. Eimura, R. Kashiwabara, T. Matsuda, Y. Isshiki, A. Hirose, Femtosecond laser peening of 2024 aluminum alloy without a sacrificial overlay under atmospheric conditions, J. Laser Appl. 29, 012005 (2017); doi: 10.2351/1.4967013

[23] ASTM E 837-08, 2008. Standard Test Method for Determining Residual Stresses by the Hole-Drilling Strain-Gage Method. ASTM Int., USA.

[24] Vishay Tech Note TN-503, 2010. Measurement of Residual Stresses by the Hole-Drilling Strain Gage Method. Vishay Precision Group, Micro Measurements Int., USA.

[25] ASTM G 99-04, 2004. Standard Test Method for Wear Testing with a Pin on Disk Apparatus. ASTM Int., USA.

[26] K.P. Shaha, Y.T. Pei, D. Martinez-Martinez, J.Th.M. De Hosson, Influence of hardness and roughness on the tribological performance of TiC/a-C nanocomposite coatings, Surface & Coatings Technology 205 (2010) 2624–2632.

[27] A. Cavaleiro, J.T.M. De Hosson, Nanostructured Coatings, Springer, New York,2006.

[28] K.P. Shaha, Y.T. Pei, D. Martinez-Martinez, J.Th.M. De Hosson, Influence of Surface Roughness on the Transfer Film Formation and Frictional Behavior of TiC/a-C Nanocomposite Coatings, Tribol. Lett. (2010).

[29] J.Z. Lu, K.Y. Luo, Y.K. Zhang, G.F. Sun, Y.Y. Gu, J.Z. Zhou, X.D. Ren, X.C. Zhang, L.F. Zhang, K.M. Chen, C.Y. Cui, Y.F. Jiang, A.X. Feng, L. Zhang, Grain refinement of LY2 aluminum alloy induced by ultra-high plastic strain during multiple laser shock processing impacts, Acta. Mater. 58 (2010) 3984–3994.

[30] I. Yakimets, C. Richard, G. Béranger, P. Peyre, Laser peening processing effect on mechanical and tribological properties of rolling steel 100Cr6. Wear 256 (2004) 311–320.

[31] C. Mansilla, D. Martínez-Martínez., V. Ocelík, J.Th.M. De Hosson, On the determination of local residual stress gradients by the slit milling method, J. Mater. Sci. 50 (2015) 3646–3655.

[32] C. Mansilla, V. Ocelík, J.Th.M. De Hosson, Local residual stress measurements on nitride layers, Materials Science&EngineeringA636 (2015) 476–483.

[33] C. Mansilla, V. Ocelík, J.Th.M. De Hosson, A New Methodology to Analyze Instabilities in SEM Imaging, Microsc. Microanal. 20 (2014) 1625–1637.

[34] I. Basu, V. Ocelík, J.Th.M. De Hosson, Measurement of spatial stress gradients near grain boundaries, Scripta Materialia 136 (2017) 11–14.

[35] N. Kashaev, V. Ventzke, M. Horstmann, S. Chupakhin, S. Riekehr, R. Falck, E. Maawad, P. Staron, N. Schell, N. Huber,Effects of laser shock peening on the microstructure and fatigue crack propagation behaviour of thin AA2024 specimens, Int. J. Fatigue 98 (2017) 223–233

[36] S. Chupakhin, N. Kashaev, N. Huber, Effect of elasto-plastic material behaviour on determination of residual stress profiles using the hole drilling method, J.Strain Anal. Eng. Des. 51/8 (2016), 572–581.

[37] C. Correa, D. Peral, J.A. Porro, M. Díaz, L. Ruiz de Lara, A. García-Beltrán, et al., Random-type scanning patterns in laser shock peening without absorbing coating in 2024-T351 Al alloy: a solution to reduce residual stress anisotropy, Opt. Laser Technol. 73 (2015) 179–187.

[38] Z. Bergant, U. Trdan, J. Grum, Effects of laser shock processing on high cycle fatigue crack growth rate and fracture toughness of aluminium alloy 6082-T651, International Journal of Fatigue 87 (2016) 444–455

[39] P. Peyre, R. Fabbro, P. Merrien, H.P. Lieurade, Laser shock processing of aluminium alloys. Application to high cycle fatigue behaviour, Mater. Sci. Eng. A 210 (1996) 102–113.

[40] S. Huang, J.Z. Zhou, J. Sheng, K.Y. Luo, J.Z. Lu, Z.C. Xu, X.K. Meng, L. Dai, L.D. Zuo, H.Y. Ruan, H.S. Chen,. Effects of laser peening with different coverage areas on fatigue crack growth properties of 6061-T6 aluminum alloy, Int. J. Fatigue 47 (2013) 292-299.

[41] J. Noordhuis, J.Th.M. De Hosson, Surface modification by means of laser melting combined with shot peening: A novel approach, Acta Mater. 40/12 (1992) 3317–3324.

[42] G.A. Edwards, K. Stiller, G.L. Dunlop, M.J. Couper, The precipitation sequence in Al–Mg–Si alloys, Acta Mater. 46 (1998) 3893–3904.

[43] R. Fabbro, P. Peyre, L. Berthe, X. Scherpereel, Physics and applications of laser shock processing. Laser. Appl. 10 (1998) 265–79.

[44] K. Hiratsuka, K. Muramoto, K, Role of wear particles in severe–mild wear transition. Wear 259 (2005) 467–476.

[45] J. Zhang, A.T. Alpas, Transition between mild and severe wear in aluminium alloys, Acta. Mater. 45 (1997) 513–528.

[46] D.K. Dwivedi, Adhesive wear behaviour of cast aluminium–silicon alloys: Overview. Mater. Design 31 (2010) 2517–2531.

[47] O. Higounenc, Correlation of shot peening parameters to surface characteristic, in: ICSP-9, Paris, France, 2005, pp28–35.

Tables

Table 1. 3D CLSM topography (roughness and waviness) results.

Sample	S_c (μm)	S_a (μm)	S_z (μm)	W_c (μm)	W_a (μm)	W_z (μm)
BM	27.860	2.689	48.629	5.240	1.098	1.986
LSP–2.5 mm	48.369	3.479	76.577	9.047	3.011	6.646
LSP–2.0 mm	66.905	4.374	85.514	21.351	8.955	14.334
LSP–2.5 mm	85.777	6.463	94.140	77.388	21.398	68.704

Table 2. Wear volume (W_v) and specific wear rate (K) results.

Sample	W_v (mm^3)	σ (mm^3)	K (mm^3/N m)	σ (mm^3/N m)
Untreated	2.041E-03	4.165E-4	4.083E-4	8.331E-5
LSP–1.5 mm	1.959E-03	3.199E-4	3.918E-4	6.398E-5
LSP–2.0 mm	1.820E-03	2.952E-4	3.640E-4	5.904E-5
LSP–2.5 mm	2.045E-03	4.289E-4	4.090E-4	8.578E-5

Figure captions

Fig. 1. Schematic presentation of the overall heat treatment and subsequent LSP treatment.

Fig. 2. (a) SEM/BEI microstructure of the base material; (b) EDS line analysis results marked on (a).

Fig. 3. Surface appearance after LSP with different beam diameters; (a) LSP–1.5 mm and (b) LSP–2.5 mm.

Fig. 4. CLSM topographical analysis of BM sample; (a) 3D image, (b) 2D image after high-pass filtration and (c) topographical line profiles marked in (b).

Fig. 5. CLSM analysis of LSP–1.5 mm sample. (a) 3D image, (b) 2D image after high-pass filtration and (c) topographical line profiles marked in (b).

Fig. 6. (a,b) In-depth residual stresses and (c) 3D presentation of the drilled blind-hole and its cross section (*Note*: blank spaces in Fig.6c represent the un-measured points).

Fig. 7. Comparison of surface residual stress and near-surface micro-hardness.

Fig. 8. TEM bright field observations of various samples: (a) BM, (b-d) LSP samples treated with different laser beam diameters.

Fig. 9. Friction coefficient as a function of sliding distance.

Fig. 10. Typical wear scar (a) and 3D CLSM wear scar profile (b).

Fig. 11. (a) Schematic presentation of roughness measurement, (b) determination of maximum width and height of the cross sectional profiles of the wear track and (c) surface profiles inside the wear track with given values obtained form the topographiyal analyses.

Fig. 12. SEM/SEI images of wear scars; (a-b) Untreated and (c-d) LSP sample treated with 2.0 mm laser beam diameter.

Fig. 13. Schematic presentation of surface topography effect on tribological behaviour under dry contact condition.